AIMS Mathematics, 9(10): 28722–28740.
DOI: 10.3934/math.20241393
Received: 10 July 2024
Revised: 18 September 2024
Accepted: 29 September 2024
Published: 10 October 2024

https://www.aimspress.com/journal/Math

Research article

An approximate analytical solution for groundwater variation in unconfined aquifers subject to variable boundary water levels and groundwater recharge

An-Ping Wang, Ming-Chang Wu, and Ping-Cheng Hsieh*

Department of Soil and Water Conservation, National Chung Hsing University, Taichung 40227, Taiwan

* **Correspondence:** Email: ida364@email.nchu.edu.tw.

Abstract: This study investigated the effects of fluctuating boundary water levels and surface recharge on groundwater flow within unconfined aquifers. We aimed to understand how changes in recharge patterns and variable boundary water levels, such as those from rivers or canals, affect groundwater levels over time and space. To achieve this, we solved the linearized Boussinesq equation using the time-marching method alongside the generalized integral transformation method. Our analysis focused on how different types of recharge affect groundwater level variations and flow dynamics. We found that boundary effects on groundwater level change propagate from the edges toward the aquifer's center, becoming more pronounced with increased boundary water levels. Over time, the system stabilizes, leading to a steady water table height and flow rate, which depend on the disparity between the boundary water levels. Our analytical model demonstrated flexibility and practical applicability by allowing for the consideration or omission of various influencing factors, thus facilitating complete knowledge about groundwater variations and offering future strategic insights for sustainable groundwater resource management.

Keywords: groundwater table; unconfined aquifer; varying boundary water level; recharge; generalized integral transform method
Mathematics Subject Classification: 76S05

1. Introduction

The study of groundwater dynamics spans centuries, yet it has never been more pertinent than in today's context of global climate change. As freshwater resources become increasingly precious, understanding and managing groundwater has become crucial to ensuring sustainable water availability [1–3]. Advanced computational technologies have revolutionized the field, enabling the development of sophisticated groundwater models. These tools have significantly deepened our understanding by simulating the intricate processes governing groundwater flow, particularly in unconfined aquifers.

A pivotal area of research has been the exploration of groundwater flow dynamics under the influence of external factors like surface recharge and boundary water level fluctuations. Noteworthy in this domain is the work in [4], which showcased the application of the Artificial Neural Network-Finite Element subsurface Flow (ANN-FEFLOW) model. This model distinguished itself by simulating groundwater flow changes in arid regions of China with an accuracy superior to traditional methods, attributing this success to its consideration of variable boundary conditions. This approach offered valuable perspectives for refining groundwater management strategies in arid landscapes. Furthermore, studies investigating the effects of ocean waves on groundwater levels have underscored the importance of accommodating varying boundary conditions. Research in [5–7] elucidated the cyclic nature of groundwater discharge and the potential risks of seawater intrusion, influenced by tidal activities and climatic factors like rainfall. These studies highlight that the bottom inclination influences the distance at which water levels change; the farther inland, the more rapid the decrease in influence. Additionally, higher rainfall intensity inhibits the tidal effect. These insights stress incorporating dynamic boundary conditions in groundwater models to accurately predict flow patterns and respond to environmental changes.

Central to these investigations is the application of the Boussinesq equation, derived from integrating Darcy's formula with the continuity equation [8–11]. This foundational equation is the cornerstone for modeling groundwater flow in unconfined aquifers, facilitating the prediction of groundwater level responses to various stimuli. Through theoretical advancements and empirical validations, research in this field continues to evolve, offering nuanced understandings of groundwater behavior in response to changing environmental conditions [12–17].

Upadhyaya and Chauhan [18] introduced several analytical and numerical methods to model groundwater level variations between two drains within a horizontal or inclined aquifer. They evaluated the accuracy of these methods by comparing predicted groundwater levels at the midpoint against experimental data. The findings indicated that the hybrid finite analytic solution outperformed others, ranking above the finite element method, the finite difference method, and the analytical linearization techniques in [19,20].

Zissis et al. [21] delineated the aquifer into areas of recharge (adjacent to the boundary river) and non-recharge. They utilized the Laplace transformation method to address the linearized Boussinesq equation, considering uniform recharge and exponential fluctuations in river water levels. Their results aligned closely with numerical solutions by the finite element method, showcasing analytical solutions' efficacy in investigating groundwater level responses to abrupt changes in adjacent river levels. Interestingly, linearizing the nonlinear Boussinesq equation had minimal effect on the predicted water level height, as found in the work in [22,23].

Sudicky [24] and Sudicky and McLaren [25] applied Laplace and Fourier transform techniques

to determine aquifer water levels before [26] explored how groundwater levels in rivers and coastal aquifers respond to environmental stimuli. Additionally, [27,28] examined the effects of water level adjustments and tidal influences on groundwater. Their sensitivity analysis indicated that riverbed leakage scarcely affects groundwater fluctuations, whereas the impact of river water levels becomes more pronounced with increased leakage.

The common simplification of river water level changes in many studies—either as instantaneous or step-like uplifts—oversimplifies these variations' complex, nonlinear, and continuous nature. This paper presents a conceptual model for the riparian aquifer system, accommodating time- and space-varying recharge. We derive analytical solutions for groundwater flow within unconfined aquifers under intricate boundary conditions, aiming to bridge the gap between simplified theoretical assumptions and the dynamic realities of groundwater systems.

2. Methodology

2.1. Conceptual and mathematical modeling

Our study investigates groundwater level changes in a horizontal unconfined aquifer with variable boundary water levels resulting from groundwater recharge after rainfall percolation. The aquifer model is a one-dimensional rectangular prism characterized by length L and height D, with recharge r on the ground surface and impermeable base. Boundary water levels are represented by $h_L(t)$ and $h_R(t)$ at the left and right edges, respectively.

Groundwater flow is governed by the mass balance equation, which, in terms of the specific yield S, groundwater level height $h(x,t)$, recharge rate $r(x,t)$, and flow rate q per unit width, is given by:

$$S\frac{\partial h}{\partial t} - r + \frac{\partial q}{\partial x} = 0. \tag{1}$$

Flow within the aquifer, adhering to Darcy's law, is defined as:

$$q = -kh\frac{\partial h}{\partial x}, \tag{2}$$

where k is the hydraulic conductivity.

Substituting Eq (2) into Eq (1) yields the Boussinesq equation with a source term r:

$$S\frac{\partial h}{\partial t} + \frac{\partial}{\partial x}\left(-kh\frac{\partial h}{\partial x}\right) = r. \tag{3}$$

Referring to the linearization techniques presented in [21,29], an average groundwater level $\overline{h}$ is suggested to replace the first h of the nonlinear term in Eq (3), enhancing it through linearization techniques to accommodate small perturbations in groundwater level compared to the average groundwater level. After assessing the applicability of the linearization parameters, the water level $h_{t'}(x)$ at an early moment by a time step is presented as a novel linearization parameter, and the time-marching method is employed to calculate it from the initial water level. The time step Δt is small enough to satisfy the assumptions of the semi-linearization technique, ensuring that the water level change between two subsequent moments varies much less than h. Thus, Eq (3) can be rearranged as follows:

$$\frac{\partial^2 h^2}{\partial x^2} = \frac{S}{k h_{t'}} \frac{\partial h^2}{\partial t} - \frac{2r}{k}, \tag{4}$$

where $h_{t'} = h(x, t - \Delta t)$ is the groundwater level at the moment before the concerned time t, and Δt is the time step.

In addition, the initial water level h_0 can be observed from the wells, and the various river water levels at both boundaries $x = 0$ and $x = L$ can be collected from the gauge station. Hence, the initial condition and boundary conditions are presumed as follows:

$$h(x, 0) = h_0(x), \tag{5}$$

$$h(0, t) \equiv h_L(t), \tag{6}$$

$$h(L, t) \equiv h_R(t). \tag{7}$$

For solving the boundary-value problem, dimensionless variables are introduced to simplify the above equations:

$$X = \frac{x}{L}, H = \frac{h^2 - {h_0}^2}{\overline{h_0}^2}, \ T = \frac{t}{t_d}, \ I(X) \equiv \frac{{h_0}^2}{\overline{h_0}^2}, \ R(X, T) \equiv \frac{r}{k}, \ Q \equiv \frac{2Lq}{k\overline{h_0}^2} = -\left(\frac{\partial H}{\partial X} + \frac{\partial I}{\partial X}\right),$$

where $\overline{h_0} = \frac{1}{L}\int_{x=0}^{L} h_0(x)dx$ and t_d is the duration of recharge.

The Boussinesq equation (4) becomes

$$\frac{\partial^2 H}{\partial X^2} = \alpha \frac{\partial H}{\partial T} - \gamma R - \frac{d^2 I}{dX^2}, \tag{8}$$

where $\alpha \equiv \frac{SL^2}{k t_d h_{t'}}, \ \gamma \equiv \frac{2L^2}{\overline{h_0}^2}$.

$$H(X, 0) = 0, \tag{9}$$

$$H(0, T) = \frac{{h_L}^2 - h_0^2(0)}{\overline{h_0}^2} \equiv H_L(T), \tag{10}$$

$$H(1, T) = \frac{{h_R}^2 - h_0^2(L)}{\overline{h_0}^2} \equiv H_R(T). \tag{11}$$

Employing the following linear transformation:

$$\Delta H(X, T) \equiv H(X, T) - [H_L(T) + (H_R(T) - H_L(T))X]. \tag{12}$$

Equations (8)–(11) become

$$\frac{\partial^2 \Delta H}{\partial X^2} = \alpha \frac{\partial \Delta H}{\partial T} - \gamma R + \alpha(1 - X)\frac{dH_L}{dT} + \alpha X \frac{dH_R}{dT} - \frac{d^2 I}{dX^2}, \tag{13}$$

$$\Delta H(X, 0) = 0, \tag{14}$$

$$\Delta H(0,T) = 0, \tag{15a}$$

$$\Delta H(1,T) = 0. \tag{15b}$$

2.2. Analytical solutions

In this study, the following transforms of the Generalized Integral Transform Method (GITM) presented in [30] are employed.

Transform formula:

$$H_T(\beta_m,T) = \int_{X'=0}^{1} K(\beta_m,X') \cdot \Delta H(X',T)\,\mathrm{d}X'. \tag{16}$$

Inverse transform formula:

$$H_T(\beta_m,T) = \int_{X'=0}^{1} K(\beta_m,X') \cdot \Delta H(X',T)\,\mathrm{d}X'. \tag{17}$$

Here, the kernel

$$K(\beta_m,X) = \sqrt{2}\sin(\beta_m X) \tag{18}$$

with $\beta_m = m\pi,\ m \in \boldsymbol{N}$ (natural number).

Applying these transformations, we reformulate the Boussinesq equation, setting up the conditions for a linear transformation to solve the equation using GITM. The transformations and inverse transformations allow us to handle complex boundary conditions dynamically. The derivation processes of ΔH in Eq (13) by GITM are shown in Appendix A.

After expanding the integral of Eq (A7) and organizing the equation, we can get:

$$\Delta H(X,T) = \sum_{m=1}^{\infty} \frac{2}{\alpha} \cdot \sin(\beta_m X)\,(F_1 + F_2 + F_3), \tag{19}$$

where

$$F_1(T) \equiv \int_{\tau=0}^{T}\int_{X'=0}^{1} \sin(\beta_m X')\,\gamma R \cdot \exp\left[\frac{-{\beta_m}^2}{\alpha}(T-\tau)\right]\mathrm{d}X'd\tau, \tag{20}$$

$$F_2(T) \equiv -\int_{\tau=0}^{T}\int_{X'=0}^{1} \sin(\beta_m X')\left(\alpha(1-X')\frac{dH_L}{d\tau} + \alpha X'\frac{dH_R}{d\tau}\right), \tag{21}$$

$$F_3(T) \equiv \int_{\tau=0}^{T}\int_{X'=0}^{1} \sin(\beta_m X') \cdot \frac{d^2 I}{dX'^2} \cdot \exp\left[\frac{-{\beta_m}^2}{\alpha}(T-\tau)\right]\mathrm{d}X'd\tau. \tag{22}$$

Each term, F_1, F_2, and F_3, represents the source term, boundary water level variations, and initial groundwater level conditions, respectively. Through GITM, we derive explicit formulas for groundwater levels and flow discharge as the following, which are then verified against numerical solutions for accuracy in the next section.

Substituting Eq (19) into Eq (12) yields

$$H(X,T) = \sum_{m=1}^{\infty} \frac{2}{\alpha} \cdot \sin(\beta_m X)\,(F_1 + F_2 + F_3) + (1-X)H_L + XH_R. \tag{23}$$

After the groundwater level has been estimated, the flow discharge at the outlet can be obtained by integrating Eq (2) as follows.

$$Q = \sum_{m=1}^{\infty} \frac{-2}{\alpha} [\beta_m \cos(\beta_m X) \cdot (F_1 + F_2 + F_3) + H_L - H_R - \frac{\partial I}{\partial X}. \tag{24}$$

3. Comparison of analytical and numerical solutions

Our approach is validated against the established analytical solution proposed in [31] and through comparison with the numerical solution developed by ourselves, using specific scenarios to test our model's accuracy and practical applicability under varying conditions of recharge and boundary water levels. The recharge of their mathematical model was presented by an exponential function, $r/k = r_0/k + r_1/k \cdot \exp(-dt)$, indicating that the river water level varies quantitatively with time. The application of Eq (20) by introducing the above exponential type recharge is given in Appendix B. The parameters used are as follows: $L = 1000$ m, $a = 12{,}000$ m^2/d, $h_0 = 0$, ${h_L}^2 - {h_0}^2 = 120$ m^2, ${h_R}^2 - {h_0}^2 = 100$ m^2, $r_0/k = 1 \times 10^{-5}$, $r_1/k = 2 \times 10^{-5}$, $d = 0.1$ 1/d, $t = 2, 5, 10$ d, $\Delta t = 0.1$ d, $\overline{h} = 72$ m, $S = 0.27$, and $k = 45$ m/d.

Regarding the linearization improvement of the governing equation, the most significant difference between this study and [31] is using the time-marching method to enhance accuracy. With minimal changes in groundwater level, the present solution closely aligns with the linear solution obtained in [31]. However, when there are substantial changes in water level, the solution in [31] becomes impractical because it must satisfy the assumption of a slight fluctuation in groundwater level. The time-marching method can provide reasonable groundwater level estimates by selecting a suitable time-step interval to ensure that the groundwater level change in each step adheres to the linearization assumption because the adjacent groundwater level change is minimal.

If the varying water levels at both boundaries also admit the change of exponential functions with constant decaying rates λ_L and λ_R, they can be expressed as follows:

$$h_L(t) = h_{L,f} - \left(h_{L,f} - h_L(0)\right) \cdot \exp(-\lambda_L \cdot t), \tag{25a}$$

$$h_R(t) = h_{R,f} - \left(h_{R,f} - h_R(0)\right) \cdot \exp(-\lambda_R \cdot t), \tag{25b}$$

where $h_{L,f}$ and $h_{R,f}$ are the equilibrium water level of rivers at the left and right boundaries, respectively. The application of Eq (21) by introducing the variable boundary water level is shown in Appendix C, and an exponential type water level distribution is shown in Appendix D. To complement our analytical solutions, a numerical scheme was employed using finite difference methods to approximate the groundwater flow equations. The aim was to validate our analytical model by comparing its predictions with those from the numerical model, especially under dynamic boundary conditions and variable recharge rates.

The derived difference expression is as follows:

$$\left(h_{i'}^{n'+1}\right)_{m'+1} = \left\{\frac{1}{2(\Delta x')^2}\left[\left(h_{i'+1}^{n'+1}\right)_{m'}^{\ 2} - 2\left(h_{i'}^{n'+1}\right)_{m'}^{\ 2} + \left(h_{i'-1}^{n'+1}\right)_{m'}^{\ 2}\right] + \frac{r_{i'}^{n'+1}}{k}\right\} \cdot \frac{k\Delta t'}{S} + h_{i'}^{n'}, \tag{26}$$

where i' and n$'$ denote the node in the space and time domain, respectively, and m' denotes the number of iterations. The condition of solution convergence is:

$$\left|\left(h_{i'}^{n'+1}\right)_{m'+1} - \left(h_{i'}^{n'+1}\right)_{m'}\right| < 10^{-3}\ \text{m} \tag{27}$$

with $\Delta x' = 5$ m and $\Delta t' = 0.0002$ d.

As depicted in Figure 1(a), the river water levels are assumed constant with the reference of [31]. In the absence of recharge, the water level is merely affected by the difference in the river water levels, and the groundwater level gradually rises from the initial water level until the water levels reach equilibrium. In Figure 1(b), the rising groundwater level depends on the recharge rate when the recharge is considered. Nevertheless, the trend is similar to the result in Figure 1(a). The present analytical solution agrees very well with [31] and the numerical solutions. Further, it provides a more concise and general solution that can be applied to various recharge and boundary water levels.

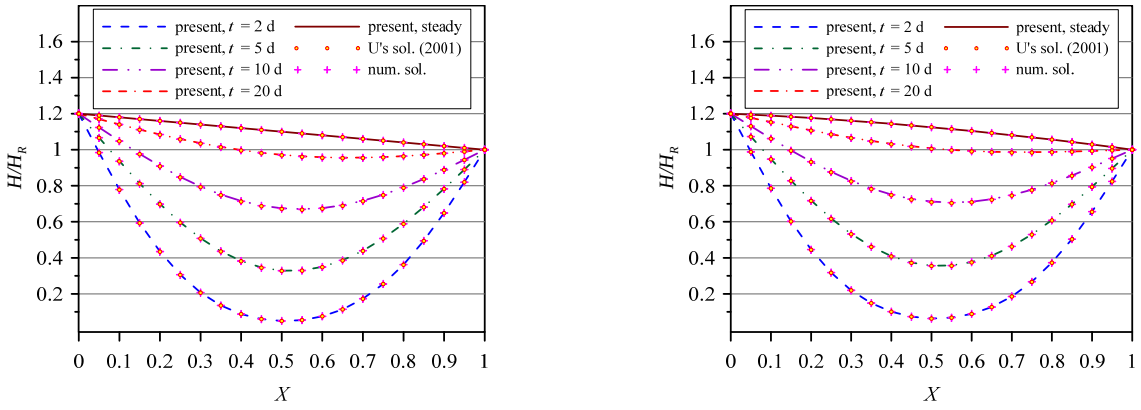

(a) Without recharge

(b) With recharge (d=0.1 1/d)

Figure 1. Comparison of changes in groundwater level with the numerical solution and the solution presented by [31] for constant boundary water levels.

Different time steps are presented to evaluate the effect of time steps on the present analytical solutions and examine the solutions' consistency, as shown in Figures 2 and 3. The parameters used are as follows: $L = 200$ m, $h_0 = 5$ m, $h_{L,f} = 6$ m, $h_{R,f} = 5.2$ m, $\lambda_L = 0.4$ 1/d, $\lambda_R = 0.4$ 1/d, $r = 0.05$ m/d, $t_d = 5$ d, $t = 1, 5, 20$ d, $S = 0.21$, and $k = 2.5$ m/d. The figures show the consistency of all solutions except choosing $\Delta t = 5$ d for the case of $t = 5$ d. It is infeasible when the simulation time and the time step are the same, resulting in a great discrepancy in the solutions. Hence, the time step size must be chosen less than the simulation time. Further, the results also indicate that the groundwater level tends to rise during the recharge period. It is evident that, due to the low hydraulic conductivity, changes of boundary water levels have minimal impact on the groundwater level in the inner region of the aquifer. The rise of groundwater level is primarily attributed to rainfall recharge. When the recharge ceases, the water level gradually stabilizes, aligning with the boundary water levels on both ends. Notably, significant differences in solutions are observed at $t = 5$ d. Comparison with the numerical solution reveals that the gap gradually widens as the recharge progresses, indicating a decrease in accuracy. Conversely, when the recharge ceases and the

groundwater level drops near the boundary ($x = 200$ m), the gap gradually narrows, increasing accuracy.

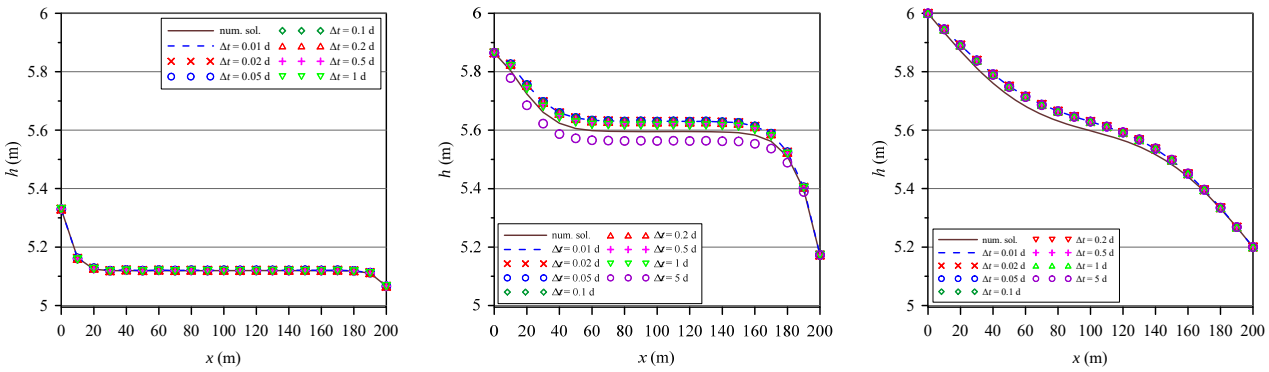

(a) $t = 1$ d (b) $t = 5$ d (c) $t = 20$ d

Figure 2. Examination of the effect of time steps on the analytical solutions for spatial changes in groundwater level at different durations.

Further, in Figure 2, the groundwater level for $x \leq 10$ m is initially affected by recharge and river water level changes, and then the groundwater level gradually increases with increasing time. After the recharge ceases, the river water level still rises, causing the groundwater level to increase slightly. Nevertheless, the groundwater level at the midsection ($x = 100$ m) remains approximately $h = 5.6$ m.

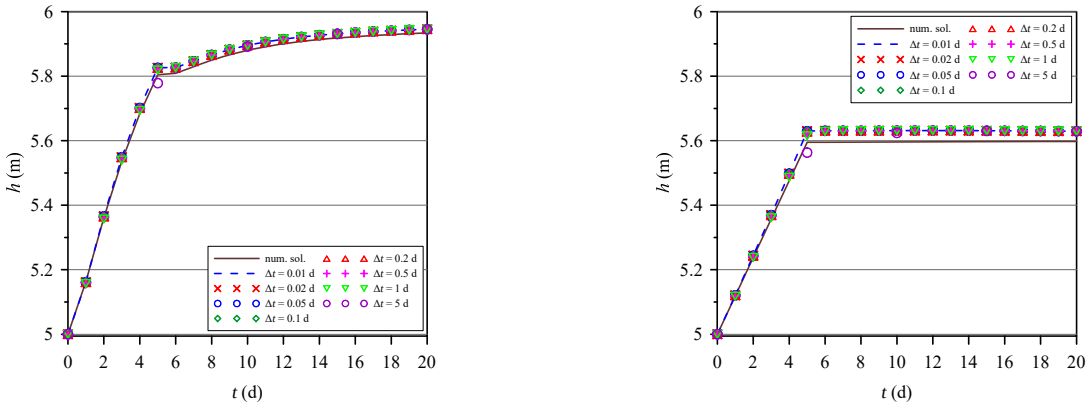

(a) $x = 10$ m (b) $x = 100$ m

Figure 3. Examination of the effect of time steps on the analytical solutions for temporal changes in groundwater level at different locations.

From Figures 2 and 3, the errors of the analytical solution and the numerical solution obtained at different simulation times and time step intervals Δt exists. Figure 4 shows the error analysis between the analytical and numerical solutions for groundwater level changes via the difference percentage $(h - h_{num})/h_{num}$ and $(h - h_{\Delta t=0.01})/h_{\Delta t=0.01}$. In Figure 4(a), using the numerical solution as a

comparison benchmark, the error of the solution of the groundwater level is the largest for both $\Delta t = 5$ d and $\Delta t = 0.01$d with a peak error of -0.675% and +0.638%, respectively, meaning that both larger and smaller time steps are inadequate. In Figure 4(b), for $\Delta t = 0.2$ d or less, the analytical solutions tend to a constant without obvious discrepancy, indicating that selecting an appropriate Δt can save computer calculation time and obtain considerable accuracy.

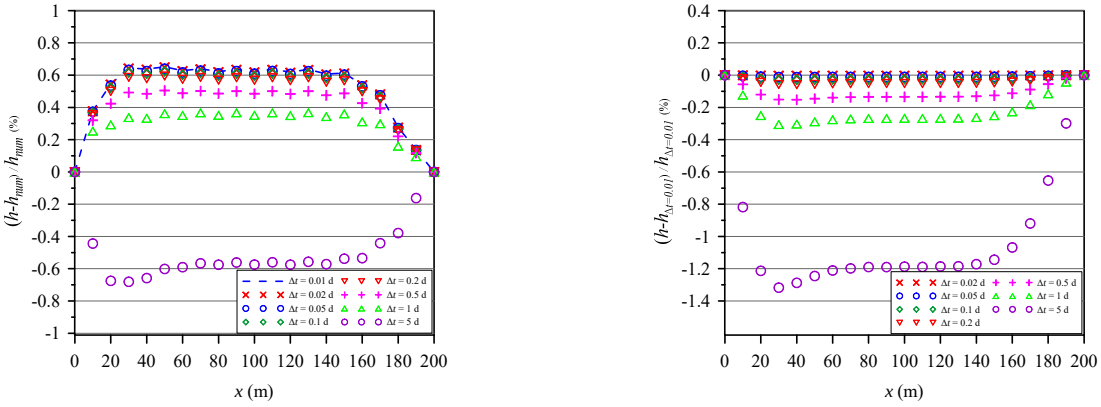

(a) (b)

Figure 4. Error analysis: (a) comparison with the numerical solutions; (b) comparison with the analytical solution using $\Delta t = 0.01$ d for different cases of time steps at $t = 5$ d.

4. Discussion

This section explores the effects of time-varying recharge patterns on groundwater levels, specifically analyzing uniform, central-peak, forward-peak, and backward-peak scenarios. The parameters guiding this investigation include a uniform initial water level function ($I = 1$), boundary water levels ($H_L = H_R = 0$), recharge duration ($T_d = 1$), study period ($T = 5$), and time step ($\Delta T = 1/48$), as elaborated in Appendix E. We modeled various recharge rates using unit step functions but maintained a consistent total recharge amount of 0.01.

During the uniform recharge period, we observed a continuous increase in groundwater level (refer to Figure 5(b)), which correspondingly heightened the flow rate at the aquifer boundaries ($X = 0$ and $X = 1$, as seen in Figure 6(b)). The central-peak pattern showed a gradual rise in groundwater level in the early half recharge period ($T < T_d/2$). Still, it accelerated after the half recharge moment ($T > T_d/2$) at the mid-recharge point ($X = 0.5$) as shown in Figure 5(b). In contrast, the forward-peak pattern demonstrated a sharp increase in the early recharge phase, followed by a deceleration (see Figure 6(a) illustrates the comparative flow rate changes). The backward-peak pattern, however, initiated a slower groundwater level increase that subsequently quickened, significantly impacting flow changes at both aquifer's ends.

Upon cessation of recharge at $T = 1$, the midpoint groundwater level change ($X = 0.5$) suggests a reduction in flow rate, potentially reaching near zero (see Figure 6(a)). Notably, the early-stage recharge predominantly dictates groundwater level changes near the boundaries post-recharge ($T > 1$). The backward-peak pattern, with its late-stage intensified recharge, results in prolonged water dissipation and elevated groundwater levels at the boundaries post-recharge cessation (Figure 5(a)).

Analyzing the recharge period ($T < 1$), the forward-peak type recorded the highest groundwater levels at $X = 0.5$, while the backward-peak type exhibited the lowest (Figure 5(b)). Interestingly, the central-peak pattern initially induced lower groundwater levels but surpassed the uniform pattern later in the recharge period. Post-recharge ($T > 1$), groundwater levels notably diverged; the backward-peak type maintained higher levels, whereas the forward-peak type resulted in lower levels, showcasing a more uniform rate of decline.

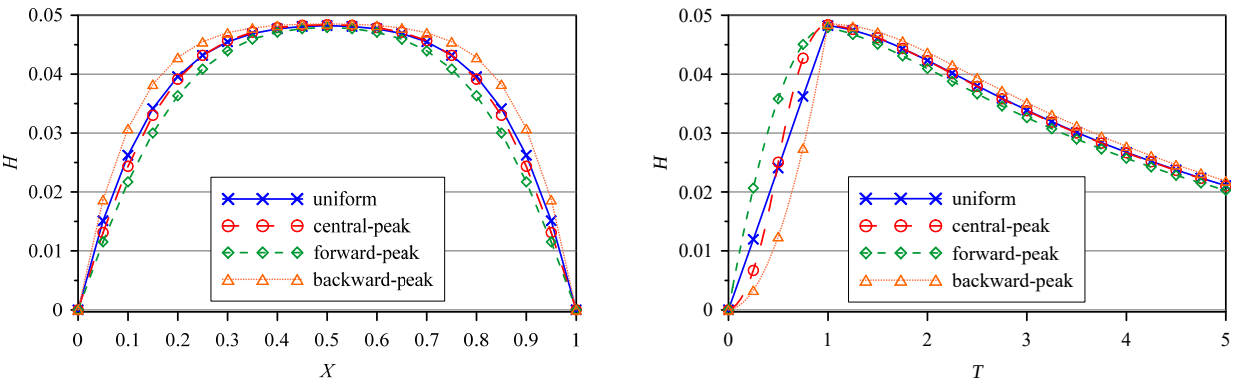

(a) T=1 (b) X=0.5

Figure 5. Variation of groundwater levels under various types of recharge.

This discussion underscores the intricate dynamics between recharge patterns and groundwater responses, offering insights into optimal recharge strategies for effective management.

Further analysis reveals that at $T = 1$, the flow rate at the midpoint is zero, as depicted in Figure 6(a). This outcome is attributed to the midpoint in a horizontal aquifer acting as a stagnation point, where the flow rate increases as water moves toward the boundaries. This phenomenon, driven by the aquifer's horizontal layout and the uniformity of recharge across space—solely dependent on time—results in an antisymmetric flow rate distribution around the midpoint. Consequently, flow rates are identical at equidistant points from the midpoint, as illustrated in Figure 6.

During the recharge period, flow rate changes—relative to a uniform recharge scenario—reflect the specific recharge patterns. For instance, the forward-peak recharge pattern accelerates the flow rate in the initial stages, whereas the backward-peak recharge pattern enhances the flow rates later in the period. This correlation between the recharge pattern and flow rate changes underscores a consistent dynamic; the flow rate intensifies over time, with the acceleration being more marked as one moves toward the boundaries. Once recharge concludes, the flow decelerates toward both ends, culminating in a stable state with smooth flow dynamics.

In practical applications, gravel piles are often utilized for groundwater recharge along certain river segments. This section investigates the alterations in groundwater flow induced by spatially dependent recharge sources, focusing on middle recharge intervals of $l_r = 0.1\,L,\ 0.2\,L,\ 0.5\,L$, and $1.0\,L$. To optimize computational efficiency, a time step of $\Delta T = 1/24$ was selected.

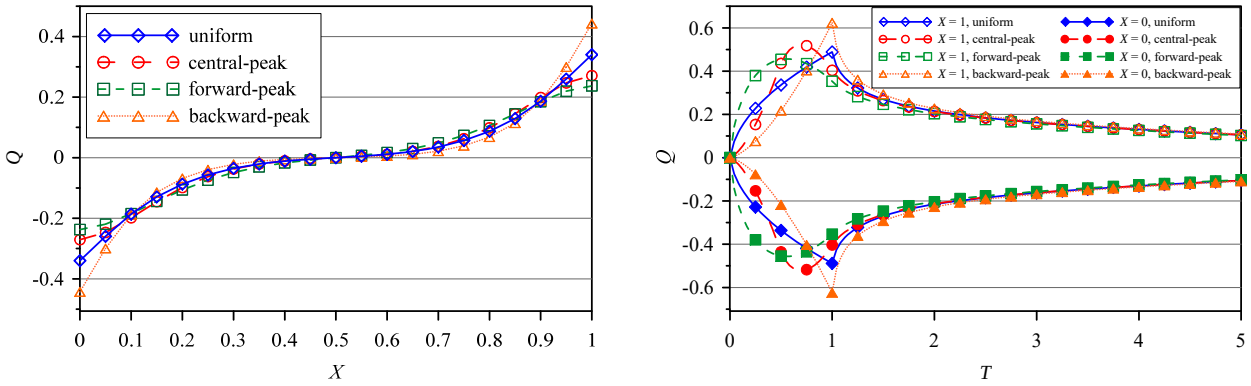

(a) T=1 (b) X=0 and X=1

Figure 6. Groundwater discharge changes for various types of recharge.

Figure 7 depicts the dimensionless changes in groundwater levels across space at two distinct times. Notably, the groundwater level variation within the recharge interval displays a characteristic curve with a descending notch, which diminishes as the recharge interval decreases. The middle recharge interval of $l_r = 0.5\,L$ proves both efficient and cost-effective for achieving the goals of groundwater recharge engineering. Moreover, analyzing the discharge variations at different recharge intervals reveals that the flow rate escalates with the interval's extension, as demonstrated in Figure 8. During the recharge period, groundwater flow accelerates toward the aquifer's extremities when the recharge interval encompasses the entire domain due to the higher gradient in the hydraulic head. Conversely, for smaller intervals ($l_r = 0.1\,L$, $0.2\,L$, and $0.5\,L$), the flow rates are significantly reduced, suggesting that the groundwater is retained within the aquifer rather than being rapidly expelled. This observation reinforces the advantage of selecting a middle recharge interval of $l_r = 0.5\,L$ for effective groundwater storage, provided the aquifer's composition supports such a strategy.

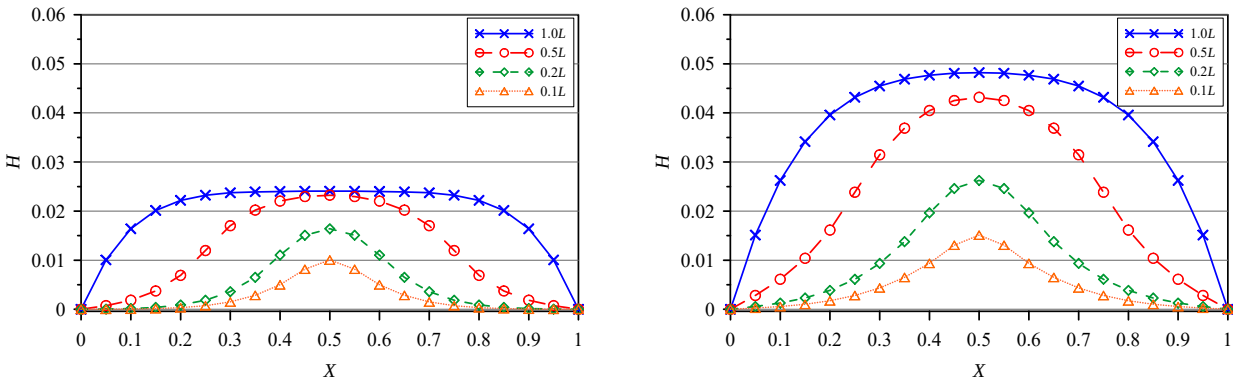

(a) T=0.5 (b) T=1

Figure 7. Spatial distribution of dimensionless groundwater levels for different spatial recharge intervals.

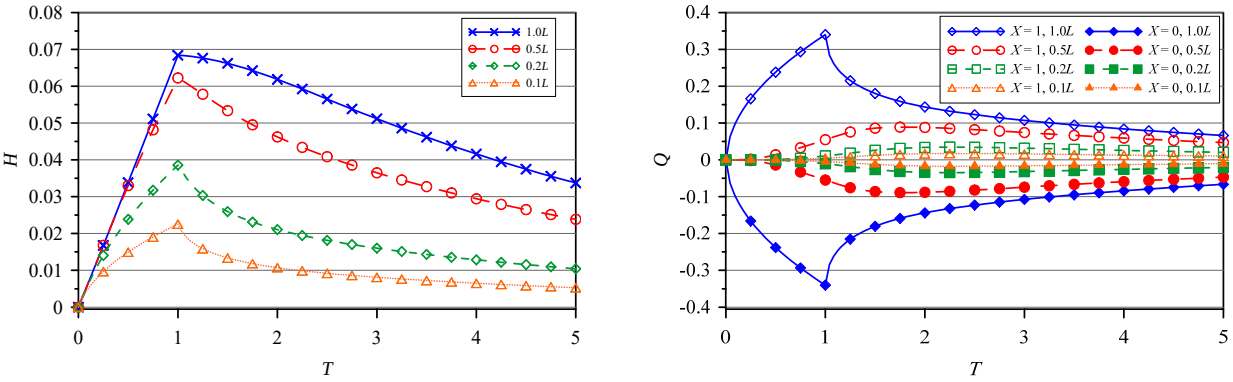

(a) X=0.5 (b) X=0, 1

Figure 8. Variation of dimensionless water level and discharge changes over time for different recharge intervals.

Figure 9 illustrates the variation in groundwater level and discharge in response to an increasing water level at the left boundary ($X = 0$) in the absence of recharge. The parameters for this analysis include a dimensionless indicator $I = 1$, left boundary equilibrium water levels $H_{L,f} = 0.1, 0.2, 0.5$, and 1.0 right boundary equilibrium water level $H_{R,f} = 0$, left boundary depth $D_L = 0.8$, and time $T = 10$. As Figure 9 reveals, the groundwater level near the active boundary experiences a noticeable increase due to the elevated river water level. This rise in groundwater level is initially swift, stabilizing at the equilibrium level relatively quickly. Beyond $T = 10$, the change in groundwater level approximates a straight line, signifying a reduction in groundwater flow discharge at $X = 0$. Conversely, at $X = 1$, there is no initial movement in the groundwater level, but discharge begins to rise incrementally as the river water level increases over a brief period. Figure 10 further details the spatiotemporal changes in the dimensionless groundwater level and discharge, providing a comprehensive view of the dynamics at play.

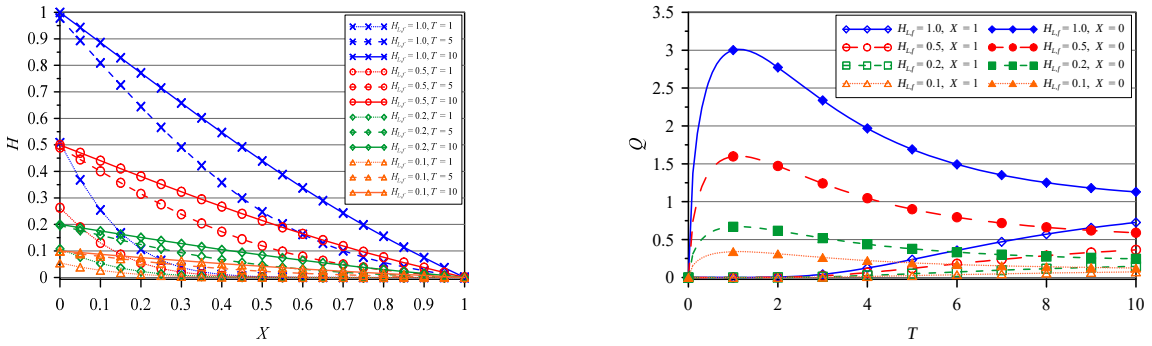

(a) T=1, 5, 10 (b) X=0, 1

Figure 9. Variations of dimensionless groundwater level and discharge changes in response to the river water level rise at $X = 0$.

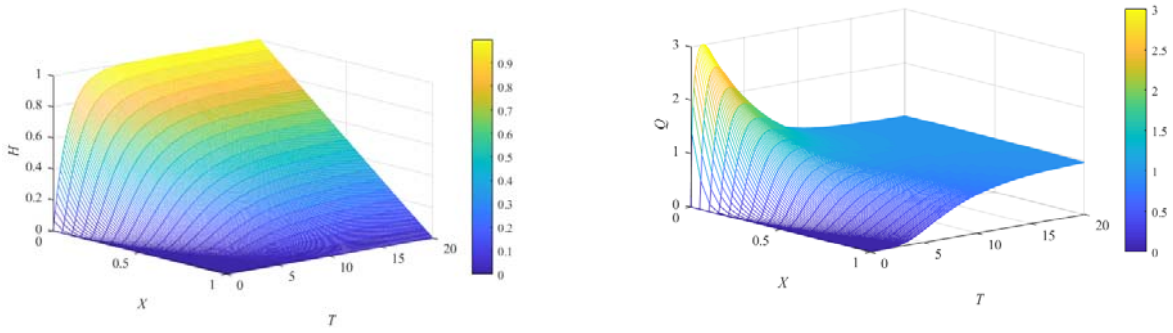

(a) H (b) Q

Figure 10. Spatiotemporal variations of the dimensionless groundwater level and discharge changes in response to the various river water levels.

5. Conclusions

This study leverages the time-marching technique to derive an analytical solution for the Boussinesq equation. Upon comparing this analytical solution with a numerical counterpart, we find that the discrepancies are minimal, underscoring the method's computational efficiency without necessitating iterative techniques. Through integrating variables such as recharge patterns, boundary water levels, and initial water levels, the study methodically investigates their effects on groundwater level and flow discharge across diverse scenarios. The key findings are as follows:

1) The analytical solutions for changes in groundwater level (H) and flow rate (Q) are categorized into three main factors: recharge, boundary water level, and initial groundwater level. This division allows for a detailed discussion of how each factor influences groundwater flow changes, enabling a clear and concise explanation of their impacts.

2) Throughout the recharge phase, the disparity between the analytical and numerical solutions incrementally increases due to variations in the governing equations. However, once the recharge ends, convergence accuracy significantly improves, with the discrepancy against numerical solutions being notably small, less than 1%. This observation highlights the analytical model's robustness and compatibility with numerical methods.

3) The change in groundwater level within the recharge interval is characterized by a curve with a distinctive downward notch. Remarkably, this notch becomes less pronounced as the recharge interval decreases. Designating the middle recharge interval to be half the aquifer's total length ($l_r = 0.5\,L$) proves to be both effective and cost-efficient, aligning well with the engineering goals of optimizing groundwater storage.

4) Alterations in the water level at the left boundary instigate water movement toward the aquifer's opposite side. Near the $X = 0$ boundary, the groundwater level initially experiences a rapid rise, swiftly achieving an equilibrium state, which, in turn, leads to a reduction in groundwater flow discharge.

These conclusions demonstrate the analytical model's versatility in accurately simulating groundwater flow changes under varied conditions, offering valuable insights for the possible strategic

management and conservation of groundwater resources.

Author contributions

An-Ping Wang: Writing – review and editing, Writing – validation, Methodology, Investigation, Formal analysis, Conceptualization. Ming-Chang Wu: Writing – review and editing, Writing – original draft, Conceptualization. Ping-Cheng Hsieh: Writing – review and editing, Methodology, Investigation, Resources, Funding acquisition. All authors have read and approved the final version of the manuscript for publication.

Use of Generative-AI tools declaration

While preparing this work, the authors used Chat-GPT and Grammarly for English editing to improve language and readability. After using this tool/service, the authors reviewed and edited the content as needed, taking full responsibility for the publication's content.

Acknowledgments

The National Science and Technology Council of Taiwan financially supported this study under Grant No. NSTC 112-2313-B-005-012.

Conflict of interest

The authors declare that they have no known competing financial interests or personal relationships that could have appeared to influence the work reported in this paper.

References

1. P. Döll, Vulnerability to the impact of climate change on renewable groundwater resources: a global-scale assessment, *Environ. Res. Lett.*, **4** (2009), 035006. https://doi.org/10.1088/1748-9326/4/3/035006
2. Y. Zhou, F. Zwahlen, Y. Wang, Y. Li, Impact of climate change on irrigation requirements in terms of groundwater resources, *Hydrogeo. J.*, **18** (2010), 1571–1582. https://doi.org/10.1007/s10040-010-0627-8
3. S. M. Gorelick, C. Zheng, Global change and the groundwater management challenge, *Water Res. Res.*, **51** (2018), 3031–3051. https://doi.org/10.1002/2014WR016825
4. Z. Huo, S. Feng, S. Kang, X. Mao, F. Wang, Numerically modelling groundwater in an arid area with ANN-generated dynamic boundary conditions, *Hydrol. Process.*, **25** (2011), 705–713. https://doi.org/10.1002/hyp.7858
5. P. Zhou, G. Li, Y. Lu, Numerical modeling of tidal effects on groundwater dynamics in a multi-layered estuary aquifer system using equivalent tidal loading boundary condition: case study in Zhanjiang, China, *Environ. Earth Sci.*, **75** (2016), 117. https://doi.org/10.1007/s12665-015-5034-y

6. P. C. Hsieh, H. T. Hsu, C. B. Liao, P. T. Chiueh, Groundwater response to tidal fluctuation and rainfall in a coastal aquifer, *J. Hydrol.*, **521** (2015), 132–140. https://doi.org/10.1016/j.jhydrol.2014.11.069
7. P. C. Hsieh, J. L. Huang, M. C. Wu, Response of groundwater levels in a coastal aquifer to tidal waves and rainfall recharge, *Water*, **12** (2020), 625. https://doi.org/10.3390/w12030625
8. W. D. Welsh, *Groundwater balance modelling with Darcy's Law*, Ph.D. Thesis, Canberra: The Australian National University, 2007.
9. H. A. Basha, Traveling wave solution of the Boussinesq equation for groundwater flow in horizontal aquifers, *Water Res. Res.*, **49** (2013), 1668–1679. https://doi.org/10.1002/wrcr.20168
10. S. N. Rai, Modeling groundwater flow in unconfined aquifers, In: S. Basu, N. Kumar, *Modelling and simulation of diffusive processes: methods and applications*, Cham: Springer, 2014, 187–210. https://doi.org/10.1007/978-3-319-05657-9_9
11. Q. Jiang, Y. Tang, A general approximate method for the groundwater response problem caused by water level variation, *J. Hydrol.*, **529** (2015), 398–409. https://doi.org/10.1016/j.jhydrol.2015.07.030
12. S. Mohan, K. Sangeeta, Recharge estimation using infiltration models, *ISH J. Hydraul. Eng.*, **11** (2005), 1–10. https://doi.org/10.1080/09715010.2005.10514796
13. D. Bui, A. Kawamura, T. Tong, H. Amaguchi, N. Nakagawa, Spatio-temporal analysis of recent groundwater-level trends in the Red River Delta, Vietnam, *Hydrogeol. J.*, **20** (2012), 1635–1650. https://doi.org/10.1007/s10040-012-0889-4
14. H. Wang, J. E. Gao, M. J. Zhang, X. H. Li, S. L. Zhang, L. Z. Jia, Effects of rainfall intensity on groundwater recharge based on simulated rainfall experiments and a groundwater flow model, *Catena*, **127** (2015), 80–91. https://doi.org/10.1016/j.catena.2014.12.014
15. M. C. Wu, P. C. Hsieh, Improved solutions to the linearized Boussinesq equation with temporally varied rainfall recharge for a sloping aquifer, *Water*, **11** (2019), 826. https://doi.org/10.3390/w11040826
16. M. C. Wu, P. C. Hsieh, Variation of groundwater flow caused by any spatiotemporally varied recharge, *Water*, **12** (2020), 287. https://doi.org/10.3390/w12010287
17. P. C. Hsieh, M. C. Wu, Changes in groundwater flow in an unconfined aquifer adjacent to a river under surface recharge, *Hydrol. Sci. J.*, (2023) 920–937. https://doi.org/10.1080/02626667.2023.2193295
18. A. Upadhyaya, H. S. Chauhan, Interaction of stream and sloping aquifer receiving constant recharge, *J. Irrig. Drain.*, **127** (2001), 295–301. https://doi.org/10.1061/(ASCE)0733-9437(2001)127:5(295)
19. P. W. Werner, On non-artesian groundwater flow, *Geofis. Pura Appl.*, **25** (1953), 37–43. https://doi.org/10.1007/BF02014053
20. P. W. Werner, Some problems in non-artesian ground-water flow, *Eos Trans. Am. Geophy.*, **38**, (1957), 511–518. https://doi.org/10.1029/TR038i004p00511
21. T. S. Zissis, I. S. Teloglou, G. A. Terzidis, Response of a sloping aquifer to constant replenishment and to stream varying water level, *J. Hydrol.*, **243** (2001), 180–191. https://doi.org/10.1016/S0022-1694(00)00415-7
22. A. Upadhyaya, H. S. Chauhan, Falling water tables in horizontal/sloping aquifer, *J. Irrig. Drain. Eng.*, **127** (2001), 378–384. https://doi.org/10.1061/(ASCE)0733-9437(2001)127:6(378)

23. A. Upadhyaya, H. S. Chauhan, Water table rise in sloping aquifer due to canal seepage and constant recharge, *J. Irrig. Drain. Eng.*, **128** (2002), 160–167. https://doi.org/10.1061/(ASCE)0733-9437(2002)128:3(160)
24. E. A. Sudicky, The Laplace transform Galerkin technique: a time-continuous finite element theory and application to mass transport in groundwater, *Water Res. Res.*, **25** (1989), 1833–1846. https://doi.org/10.1029/WR025i008p01833
25. E. A. Sudicky, R. G. McLaren, The Laplace transform Galerkin technique for large-scale simulation of mass transport in discretely fractured porous formations, *Water Res. Res.*, **28** (1992), 499–514. https://doi.org/10.1029/91WR02560
26. K. Y. Kim, T. Kim, Y. Kim, N. C. Woo, A semi-analytical solution for groundwater responses to stream-stage variations and tidal fluctuations in a coastal aquifer, *Hydrol. Process.*, **21** (2007), 665–674. https://doi.org/10.1002/hyp.6255
27. K. A. R. Kpegli, S. E. van der Zee, A. Alassane, G. Bier, M. Boukari, A. Leijnse, et al., Impact of hydraulic and storage properties on river leakage estimates: A numerical groundwater flow model case study from southern Benin, *J. Hydrol.*, **19** (2018), 136–163. https://doi.org/10.1016/j.ejrh.2018.07.004
28. L. Min, P. Y. Vasilevskiy, P. Wang, S. P. Pozdniakov, J. Yu, Numerical approaches for estimating daily river leakage from arid ephemeral streams, *Water*, **12** (2020), 499. https://doi.org/10.3390/w12020499
29. J. Bear, C. Braester, On the flow of two immscible fluids in fractured porous media, *Dev. Soil Sci.*, **2** (1972), 177–202. https://doi.org/10.1016/S0166-2481(08)70538-5
30. M. N. Özisik, *Boundary value problems of heat conduction*, New York: Dover Publications Inc., 1968.
31. A. Upadhyaya, H. S. Chauhan, Water table fluctuations due to canal seepage and time varying recharge, *J. Hydrol.*, **244** (2001), 1–8. https://doi.org/10.1016/S0022-1694(00)00328-0

Appendix

Appendix A. Derivation processes of ΔH in Eq (19) by GITM

$$\int_{X'=0}^{1} K(\beta_m, X') \cdot \frac{\partial^2 \Delta H}{\partial X'^2} \mathrm{d}X' = \int_{X'=0}^{1} K(\beta_m, X') \cdot \alpha \frac{\partial \Delta H}{\partial T} \mathrm{d}X' + \int_{X'=0}^{1} K(\beta_m, X') \cdot (-\gamma R + \alpha(1 - X') \frac{dH_L}{dT} + \alpha X' \frac{dH_R}{dT} - \frac{d^2 I}{dX'^2}) \mathrm{d}X'. \tag{A1}$$

The second-order differential term can be performed by taking integration by parts twice and the following results can be obtained:

$$\int_{X'=0}^{1} K(\beta_m, X') \cdot \frac{\partial^2 \Delta H}{\partial X'^2} \mathrm{d}X' = -\beta_m{}^2 H_T. \tag{A2}$$

Substituting Eq (A2) into Eq (A1) yields

$$\frac{dH_T}{dT} + \frac{\beta_m{}^2}{\alpha} H_T = \frac{-\delta}{\alpha}, \tag{A3}$$

where

$$\frac{dH_T}{dT} = \int_{X'=0}^{1} K(\beta_m, X') \cdot \frac{\partial \Delta H}{\partial T} dX' = \frac{\partial}{\partial T}\left(\int_{X'=0}^{1} K \cdot \Delta H \, dX'\right), \tag{A4}$$

$$\delta(T) \equiv \int_{X'=0}^{1} K(\beta_m, X') \left(-\gamma R + \alpha(1 - X')\frac{dH_L}{dT} + \alpha X' \frac{dH_R}{dT} - \frac{d^2 I}{dX'^2}\right) dX'. \tag{A5}$$

The solution to Eq (A3) can be found by multiplying the integrating factor $\frac{-\beta_m{}^2}{\alpha} T$ as follows:

$$H_T = \exp(\tfrac{-\beta_m{}^2}{\alpha} T) \cdot \int_{\tau=0}^{T} \tfrac{-\delta(\tau)}{\alpha} \cdot \exp(\tfrac{\beta_m{}^2}{\alpha} \tau) d\tau. \tag{A6}$$

Then, taking the inverse transform to Eq (A6), we can obtain

$$\Delta H(X, T) = \textstyle\sum_{m=1}^{\infty} \sqrt{2} \sin(\beta_m X) \cdot \exp(\tfrac{-\beta_m{}^2}{\alpha} T) \cdot \int_{\tau=0}^{T} \tfrac{-\delta}{\alpha} \cdot \exp(\tfrac{\beta_m{}^2}{\alpha} \tau) d\tau. \tag{A7}$$

Substituting Eq (A5) into Eq (A7) results in Eq (19).

Appendix B. Derivation of the source term $F_1(T)$ in Eq (20) by introducing an exponential type recharge

$$r(t) = r_0 + r_1 \exp(-dt), \tag{B1}$$

where r_0 and r_1 are constants.

Taking the dimensionless transformation for Eq (B1) yields

$$R(T) = R_0 + R_1 \exp(-DT), \tag{B2}$$

with $D \equiv d \cdot t_d$, $R_0 \equiv \frac{r_0}{k}$, and $R_1 \equiv \frac{r_1}{k}$.

Substituting Eq (B2) into Eq (20) yields

$$\begin{aligned} F_1(T) &= -\int_{\tau=0}^{T} \int_{X'=0}^{1} \sin(\beta_m X') \cdot \gamma [R_0 + R_1 \exp(-D\tau)] \cdot \exp\left[\frac{-\beta_m{}^2}{\alpha}(T - \tau)\right] \mathrm{d}X' d\tau \\ &= \tfrac{\alpha\gamma(\cos\beta_m - 1)}{\beta_m{}^3} \cdot [R_0 \cdot (1 - \exp(\tfrac{-\beta_m{}^2}{\alpha} T)) + \tfrac{\beta_m{}^2}{\alpha} R_1 \tfrac{\exp(-DT) - \exp(\frac{-\beta_m{}^2}{\alpha} T)}{-D + \frac{\beta_m{}^2}{\alpha}}]. \end{aligned} \tag{B3}$$

Appendix C. Derivation of the variable boundary water level term $F_2(T)$ in Eq (21)

$$\begin{aligned} F_2 &= \int_{\tau=0}^{T} \int_{X'=0}^{1} \alpha \sin(\beta_m X') \cdot \left\{(1 - X')\frac{dH_L}{d\tau} + X' \tfrac{dH_R}{d\tau}\right\} \cdot \exp\left(\frac{-\beta_m{}^2}{\alpha}(T - \tau)\right) \mathrm{d}X' d\tau \\ &= \tfrac{\alpha}{\beta_m} \textstyle\int_{\tau=0}^{T} (\frac{dH_L}{d\tau} - \cos\beta_m \frac{dH_R}{d\tau}) \cdot \exp(\frac{-\beta_m{}^2}{\alpha}(T - \tau)) d\tau. \end{aligned} \tag{C1}$$

After performing the integral over the space and then performing integration by parts, Eq (C1) becomes

$$F_2 = \frac{\alpha}{\beta_m}\left[(H_L - \cos\beta_m H_R)\cdot \exp\left(\frac{-{\beta_m}^2}{\alpha}(T-\tau)\right)\right|_{\tau=0}^{T} - \int_{\tau=0}^{T} \frac{{\beta_m}^2}{\alpha}(H_L - \cos\beta_m H_R)\cdot \exp\left(\frac{-{\beta_m}^2}{\alpha}(T-\tau)\right)d\tau] \quad \text{(C2)}$$

$$= \frac{\alpha}{\beta_m}[H_L(T) - \cos\beta_m H_R(T) - \int_{\tau=0}^{T}\frac{{\beta_m}^2}{\alpha}\left(H_L(\tau) - \cos\beta_m H_R(\tau)\right)\cdot \exp(\frac{-{\beta_m}^2}{\alpha}(T-\tau))d\tau].$$

Appendix D. Derivation of the variable boundary water level term $F_2(T)$ in Eq (21) by introducing an exponential type water level distribution (Zissis et al., 2001)

$$h_L(t) = h_{L,f} - \left(h_{L,f} - h_L(0)\right)\cdot \exp(-\lambda_L \cdot t), \quad \text{(D1)}$$

$$h_R(t) = h_R(0) = h_{R,f}, \quad \text{(D2)}$$

where $h_{L,f}$ and $h_{R,f}$ are the stable boundary water level. λ_L is the rate of the boundary water level.

Eq (D1) can be obtained after taking the dimensionless transformation:

$$H_L = G_{L1} + G_{L2}\cdot \exp(-D_L T) + G_{L3}\cdot \exp(-2D_L T), \quad \text{(D3)}$$

where

$$G_{L1} \equiv \frac{1}{\overline{h_0}^2}({h_{L,f}}^2 - {h_L}^2(0)), \quad \text{(D4)}$$

$$G_{L2} \equiv \frac{1}{\overline{h_0}^2}[-2h_{L,f}(h_{L,f} - h_L(0))], \quad \text{(D5)}$$

$$G_{L3} \equiv \frac{1}{\overline{h_0}^2}(h_{L,f} - h_L(0))^2, \quad \text{(D6)}$$

$$D_L \equiv \lambda_L t_d. \quad \text{(D7)}$$

Substituting Eq (D3) into Eq (21) yields

$$F_2 = \frac{\alpha}{\beta_m}\left[\frac{-D_L G_{L2}}{\frac{{\beta_m}^2}{\alpha} - D_L}\cdot\left(\exp(-D_L T) - \exp(\frac{-{\beta_m}^2}{\alpha}T)\right) - \frac{2D_L G_{L3}}{\frac{{\beta_m}^2}{\alpha} - 2D_L}\cdot\left(\exp(-D_L T) - \exp(\frac{-{\beta_m}^2}{\alpha}T)\right)\right]. \quad \text{(D8)}$$

Appendix E. Assumed distribution of the initial water level $I(X)$ over space

Assuming that the river water levels at both boundaries are fixed and there is no recharge for a long period, the initial groundwater level has reached a stable state and can be expressed as:

$$h_0{}^2 = C_1 x + C_2, \tag{E1}$$

with C_1 and C_2 being the undetermined coefficients.

Using the dimensionless factors for Eq (E1), the dimensionless form of the initial groundwater level becomes

$$I(X) = \frac{C_1 L}{\overline{h_0}^2} X + \frac{C_2}{\overline{h_0}^2}. \tag{E2}$$

From Eq (9), we can get:

$$I(0) = \frac{h_L{}^2(0)}{\overline{h_0}^2}, \tag{E3}$$

$$I(1) = \frac{h_R{}^2(0)}{\overline{h_0}^2}. \tag{E4}$$

After substituting Eqs (E3) and (E4) into Eq (E2), the distribution of the initial water level can be obtained as:

$$I(X) = \left(\frac{h_R{}^2(0) - h_L{}^2(0)}{\overline{h_0}^2}\right) X + \frac{h_L{}^2(0)}{\overline{h_0}^2}. \tag{E5}$$